Chem

Article

Flexibility-frustrated porosity for enhanced selective CO_2 adsorption in an ultramicroporous metal-organic framework

Graphical abstract

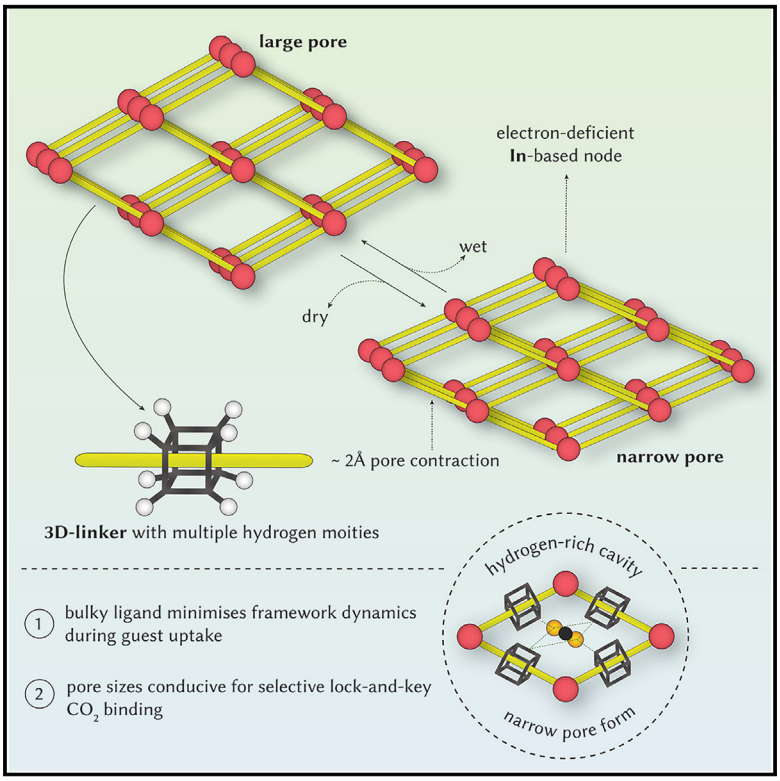

Highlights

- Established fine control over the flexibility and pore size of an ultramicroporous MOF
- Realized a cavity for selective CO_2 binding via multiple hydrogen-bonding interactions
- Mechanistic insights from *in situ* synchrotron studies and molecular simulations
- Excellent CO_2 selectivity up to 80% relative humidity

Authors

Xu Chen, Dhruv Menon, Xiaoliang Wang, ..., Sihai Yang, Omar K. Farha, David Fairen-Jimenez

Correspondence

sihai.yang@pku.edu.cn (S.Y.), o-farha@northwestern.edu (O.K.F.), df334@cam.ac.uk (D.F.-J.)

In brief

We rationalize a design strategy for developing a highly confined pore environment in a metal-organic framework (CU-4) for achieving excellent performance for the selective capture of CO_2. Advanced characterization techniques coupled with molecular simulations reveal that CU-4 exclusively recognizes CO_2 via multiple hydrogen-bonding interactions while displaying high working capacity. CU-4 maintains its performance even at high relative humidity, suggesting applicability for post-combustion capture. These concepts can be extended to achieve highly selective pore environments for the separation of challenging gaseous mixtures.

Chen et al., 2025, Chem *11*, 102382
July 10, 2025
https://doi.org/10.1016/j.chempr.2024.11.020

CellPress

Chem

CellPress
OPEN ACCESS

Article

Flexibility-frustrated porosity for enhanced selective CO_2 adsorption in an ultramicroporous metal-organic framework

Xu Chen,[1,9] Dhruv Menon,[1,9] Xiaoliang Wang,[2] Meng He,[3,6] Mohammad Reza Alizadeh Kiapi,[1] Mehrdad Asgari,[1] Yuexi Lyu,[1] Xianhui Tang,[2] Luke L. Keenan,[5] William Shepard,[4] Lik H. Wee,[1] Sihai Yang,[3,7,*] Omar K. Farha,[2,8,*] and David Fairen-Jimenez[1,10,*]

[1]Department of Chemical Engineering & Biotechnology, University of Cambridge, Philippa Fawcett Drive, Cambridge CB3 0AS, UK
[2]Department of Chemistry and International Institute for Nanotechnology (IIN), Northwestern University, Evanston, IL 60208, USA
[3]Department of Chemistry, The University of Manchester, Manchester M13 9PL, UK
[4]Synchrotron SOLEIL-UR1, L'Orme des Merisiers, Départementale 128, 91190 Saint-Aubin, France
[5]Diamond Light Source Ltd., Harwell Science and Innovation Campus, Chilton, Didcot OX11 0DE, UK
[6]European Synchrotron Radiation Facility, 71 Avenue des Martyrs, CS40220, 38043 Grenoble Cedex 9, France
[7]College of Chemistry and Molecular Engineering, Beijing National Laboratory for Molecular Sciences, Peking University, Beijing 100871, China
[8]Department of Chemical and Biological Engineering, Northwestern University, Evanston, IL 60208, USA
[9]These authors contributed equally
[10]Lead contact
*Correspondence: sihai.yang@pku.edu.cn (S.Y.), o-farha@northwestern.edu (O.K.F.), df334@cam.ac.uk (D.F.-J.)
https://doi.org/10.1016/j.chempr.2024.11.020

THE BIGGER PICTURE In the current context of global warming, the selective capture of carbon dioxide (CO_2) from point-source, industrial gaseous streams—containing a mixture of CO_2, nitrogen (N_2), and water—is vital for controlling emissions from fossil fuel combustion before they can be substituted by renewable energy. Although adsorbent-based technologies, such as those based on metal-organic frameworks (MOFs), offer potentially productive pathways for the selective capture of CO_2 from gaseous mixtures, their development is limited by the sub-angstrom differences in sizes of CO_2 and N_2 and the competitive adsorption of water. Here, we demonstrate a materials design strategy by leveraging "frustrated" framework flexibility to realize an optimum confined pore environment that selectively recognizes CO_2 while displaying a high working capacity. Using synchrotron-based X-ray diffraction experiments and molecular simulations, we are able to show that in its narrow pore configuration, our reported MOF is able to exclusively recognize CO_2 in a lock-and-key manner. Notably, the selective binding of CO_2 is maintained even at high relative humidity values, suggesting applicability for post-combustion capture—which accounts for 30% of global carbon emissions. The concept of frustrated flexibility can be extended to achieve highly selective pore environments for the separation of challenging gaseous mixtures.

SUMMARY

Selective CO_2 capture from industry is crucial for reducing emissions from fossil fuel combustion. Flexible metal-organic frameworks (MOFs) have shown promise for CO_2 adsorption via differential binding and size-exclusion mechanisms. However, achieving precise pore-size control to selectively capture CO_2, particularly in the presence of N_2 and water, remains a challenge. Here, we demonstrate a strategy for frustrating framework flexibility in a MOF to create an optimal, confined pore environment that enhances selective CO_2 recognition while maintaining high working capacity. We designed a flexible MOF, Cambridge University (CU)-4, by using a bulky cubane-derived ligand and In^{3+} ions that undergo dynamic breathing with a 2 Å contraction upon solvent exchange and removal. *In situ* synchrotron X-ray diffraction and molecular simulations reveal that the stable narrow-pore configuration creates a hydrogen-rich cavity that selectively binds CO_2 via multiple hydrogen bonds. This physisorption-based CO_2 recognition remains effective even at 80% humidity, making CU-4 promising for post-combustion carbon capture.

INTRODUCTION

The increasing levels of atmospheric carbon dioxide (CO_2) represent one of the most pressing global environmental concerns because they contribute significantly to global warming and climate change.[1,2] Before the energy transition can take place through renewable energy, technologies that effectively capture and store CO_2 from fossil fuels are necessary for reducing the environmental footprint of our current energy usage.[3] Traditional industrial CO_2 capture methods, such as liquid amines[4–6] that absorb CO_2 from flue gases through chemical interactions, are widely used. However, as a consequence of the aqueous nature of the process, they face critical limitations, including high energy requirements due to the harsh conditions required for their regeneration, increased costs, and equipment corrosion.[7,8] Adsorption-based approaches, employing solid adsorbents utilizing either physisorption or chemisorption for selective CO_2 binding, are able to overcome many of these challenges, offering promising CO_2 uptake metrics mostly because of the milder energy requirements. In other words, operating expenses are expected to be much lower than amines.[9,10] While chemisorption-based techniques in solid and porous materials—in most cases—offer high selectivity by strongly binding to CO_2 even in the presence of nitrogen (N_2) and moisture, they still carry a high energy penalty for regeneration.[11] By contrast, although typically less selective—especially in the presence of water—physisorption-based CO_2 capture requires a lower energy penalty for regeneration, leading to an overall better performance.[12]

Because of their high degree of tunability, metal-organic frameworks (MOFs) have emerged as promising candidates for carbon capture.[13,14] Their customizable nature allows for the fine-tuning of their building blocks, pore dimensions, surface chemistry, and functionalities for optimizing CO_2 adsorption[14,15] beyond that permitted by conventional materials, such as zeolites, even more in the presence of moisture.[4,12] In realistic CO_2 capture scenarios—especially post-combustion—there is a need to selectively capture CO_2 from a gaseous stream.[15] In such scenarios, enhancing the CO_2 selectivity versus N_2 and moisture during a molecular-recognition adsorption process relies on the fundamental understanding of the host-guest chemistry and the interactions that arise therein.[16,17] To achieve high-performance molecular-recognition adsorbents, it becomes essential to rationally design such systems with cooperative interactions that promote the selective uptake of targeted molecules.[16,18,19] However, enhancing selectivity through finely controlling the molecular sieving effects of rigid MOFs often compromises the working capacity of the framework, leading to a tradeoff between the working capacity and selectivity. This is because high selectivities typically demand narrow porosities, which come at the cost of reduced pore volumes, resulting in lower adsorption capacities. An area less explored within the context of addressing this limitation for the creation of optimal molecular-recognition systems is framework flexibility.[20–23] Flexible MOFs show reversible, structural changes in response to external stimuli,[24] such as variations in gas exposure, temperature, and pressure, demonstrating the ability to adjust their pore sizes, binding sites, and breathing behavior. Flexible MOFs respond to stimuli in that they exhibit behaviors such as breathing, swelling, subnetwork displacement, and linker rotation.[22] The first three examples are usually associated with changes in the unit cell volume, whereas linker rotation typically does not result in any such change.[25] For instance, a representative phenomenon in this context is the adsorption-induced gate-opening/closing behavior frequently observed in flexible MOFs, such as X-dia-1-Ni, when they reach a certain gas pressure.[26] Broadly speaking, flexible MOFs show great potential to enhance separation efficiency, even for the most challenging gas mixtures.[15,27] This ability to finely tailor MOFs' structures, pore sizes, and pore windows has allowed the simultaneous improvement of working capacity and selectivity.[15] Despite their clear potential for gas separations, the effective control of the structural flexibility of MOFs for targeted applications remains a challenge.[20,24] In particular, once framework flexibility has been leveraged for the creation of an optimal pore environment, it is desirable to restrict further framework dynamics during subsequent guest uptake.

Until now, linkers and linker functionality have shown an impact on framework flexibility.[28,29] In one approach, when considering the exploitation of linker rotation in particular,[22] several studies have focused on minimizing the structural dynamics by incorporating bulky 3D-ditopic ligands in MOF construction. For example, ditopic ligands, such as *p*-carborane-1,12-dicarboxylate, bicyclo [2.2.2]octane-1,4-dicarboxylate, and bicyclo[1.1.1]pentane-1,3-dicarboxylic acid, were employed to restrict breathing behavior and pore contraction while preserving the large-pore configuration.[30–33] This strategy proved advantageous for applications requiring the separation of similarly sized molecules, including isomers.[30–33] In addition to the linkers, the metal nodes serve as another platform for controlling the flexibility of MOFs.[34–36] For example, in the case of MIL-53(M) series, where M represents a metal such as Cr, Sc, Al, or In, the electrons of metal ions within the $[M(OH)_2O_4]$ chains influence the distance between adjacent metal ions, thereby affecting the framework's overall elongation and contraction.[36] Specifically, the large-pore configuration of Cr- and Al-based MIL-53 is stable across the tested temperatures,[37,38] whereas the Sc- and In-based MIL-53 typically stabilize in the narrow-pore configuration upon solvent removal.[39] A similar scenario can be observed in paddlewheel-based pillared-layered MOFs,[35] where the Zn-based MOFs tend to form narrower phases than the Cu-based MOF upon desolvation. The authors attributed it to the minor distortion of the stiffer Cu^{2+} coordination sphere. Recently, the rigid cubane-based 3D-ditopic linker was employed for synthesizing the aluminum-based MOF ZUL-C2,[40] which achieved C_2H_6/CH_4 and C_3H_8/CH_4 selectivities of 82 and 741 at 100 kPa, respectively. These results outperform those of some existing porous materials, such as BSF-1[41] and BSF-2.[42] In that work, ZUL-C2 maintained a rigid structure by retaining its large-pore integrity under various gas adsorption experiments. Conversely, although a contracted narrow pore might reduce the gas adsorption capacity because of a lower pore volume, it could significantly enhance selectivity. Here, suppressing the expansion of the narrow-pore configuration can restrict the flexibility of MOFs to achieve high selectivity for target gas molecules. In our study, we hypothesized that the introduction of electron-deficient In^{3+} would facilitate the distortion of the octahedral coordination sphere within $[In(OH)_2O_4]$ and therefore affect the

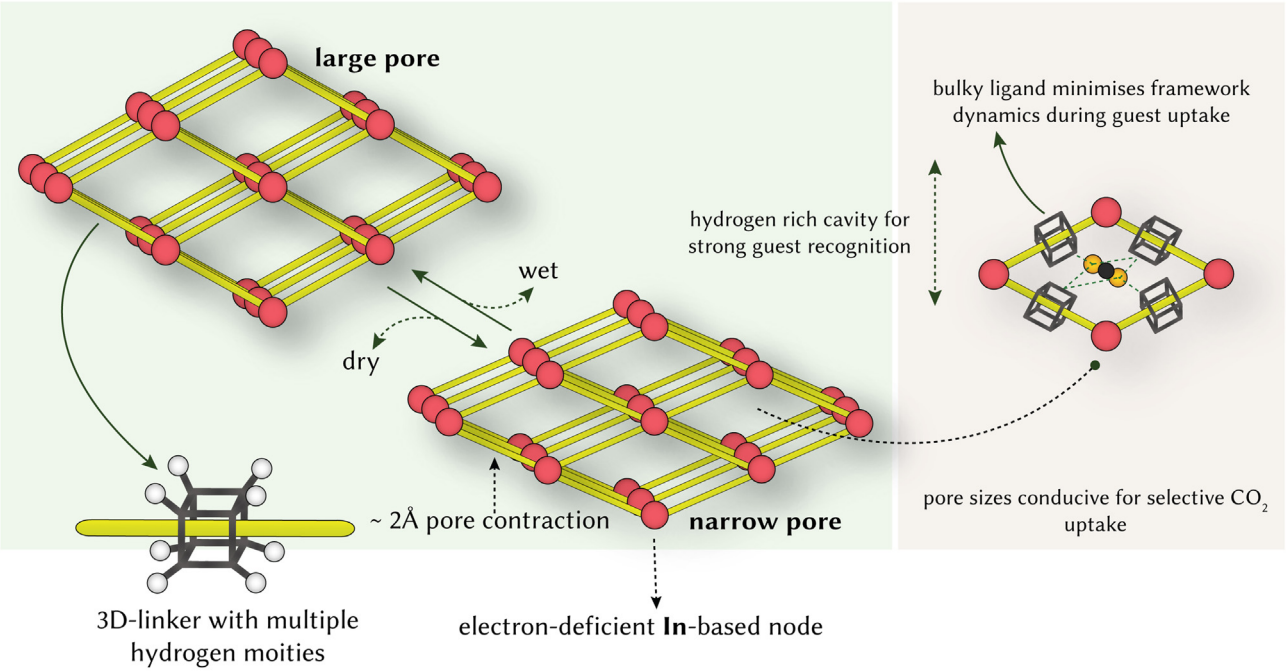

Scheme 1. Flexibility-induced strengthening of host-guest interactions

Framework flexibility resulting in a pore contraction leads to a hydrogen-rich pore cavity facilitating strong host-guest interactions, boosting selectivity. Once in its stable narrow-pore configuration, the bulky ligand minimizes framework dynamics during guest uptake—thereby inducing a frustrated state.

distance between adjacent In ions to improve the selectivity of CO_2 adsorption.

The understanding of the major factors influencing framework flexibility allows us to envision here the development of a confined pore environment that would strengthen the CO_2-framework interactions. Simultaneously, for such a material, designing a framework with pore window sizes that are favorable for CO_2 uptake but not for N_2 can also help to boost selectivity.[43] Since the kinetic diameters of CO_2 and N_2 are 3.30 and 3.64 Å, respectively,[44] a pore aperture within this range is ideal but challenging. With these considerations in mind, we demonstrate here a strategy for designing a hydrogen-confined pore environment for the selective recognition of CO_2 by exploiting frustrated framework flexibility. Our definition of "frustrated flexibility" (or "flexibility-frustrated porosity") slightly deviates from the previous example,[45] where the frustrated flexibility was introduced through precise chemical functionalization of organic ligands, resulting in some degree of structural distortion. We shift focus toward manipulating the building metal nodes that are likely to stabilize in a narrow-pore phase. We incorporated a 3D-bulky organic ligand that can minimize framework dynamics during guest uptake in the narrow-pore phase, thereby facilitating high selectivity by exploiting sub-angstrom differences in sizes (Scheme 1). Through the rational design of a flexible, channel-based, MIL-53-type, ultramicroporous MOF, **CU-4** (CU stands for Cambridge University), we achieved precise control over pore contraction by combining electron-deficient In^{3+} and the bulky 3D cubane-derived ligand. **CU-4** exhibits a pore-independent dynamic breathing behavior upon solvent exchange and removal,[25] leading to pore aperture contraction by ca. 2 Å. We hypothesized that this induced flexibility would facilitate the modulation of the hydrogen-confined pore environment to create rich adsorption pockets with multiple hydrogen-bonding (H-bonding) interactions suited to the exclusive recognition of CO_2 molecules (Scheme 1). However, once the MOF adopts this narrow-pore configuration, the presence of a bulky ligand would minimize framework dynamics during guest uptake—thereby existing in a frustrated state. As a result, the activated **CU-4**, characterized by its narrow-pore structure, shows outstanding CO_2/N_2 separation efficiency with moderate heats of adsorption (Q_{st} = 36.9 kJ/mol) for CO_2 and ideal adsorbed solution theory (IAST) selectivity of 241 for binary CO_2/N_2 mixtures (15/85, v/v). **CU-4** maintains excellent water stability and, as a result of these multiple H-bonding interactions, shows impressive CO_2 separation performance even at high relative humidity (RH) levels (up to 80% RH), alongside excellent recyclability confirmed by dynamic breakthrough tests. Notably, we observed the creation of adsorption pockets due to pore narrowing of the structure by a combination of *in situ* synchrotron X-ray diffraction and molecular simulation, which showcased the formation of multiple H bonds with CO_2 molecules. **CU-4** and, more broadly, the strategy presented herein emerge as a step toward the design of new, physisorption-based materials for carbon capture.

RESULTS AND DISCUSSION

Design and characterization

Heating cubane-1,4-dicarboxylic acid (**H_2L**) and $In(NO_3)_3$ ●$6H_2O$ in a mixture of dimethylformamide (DMF) and HNO_3

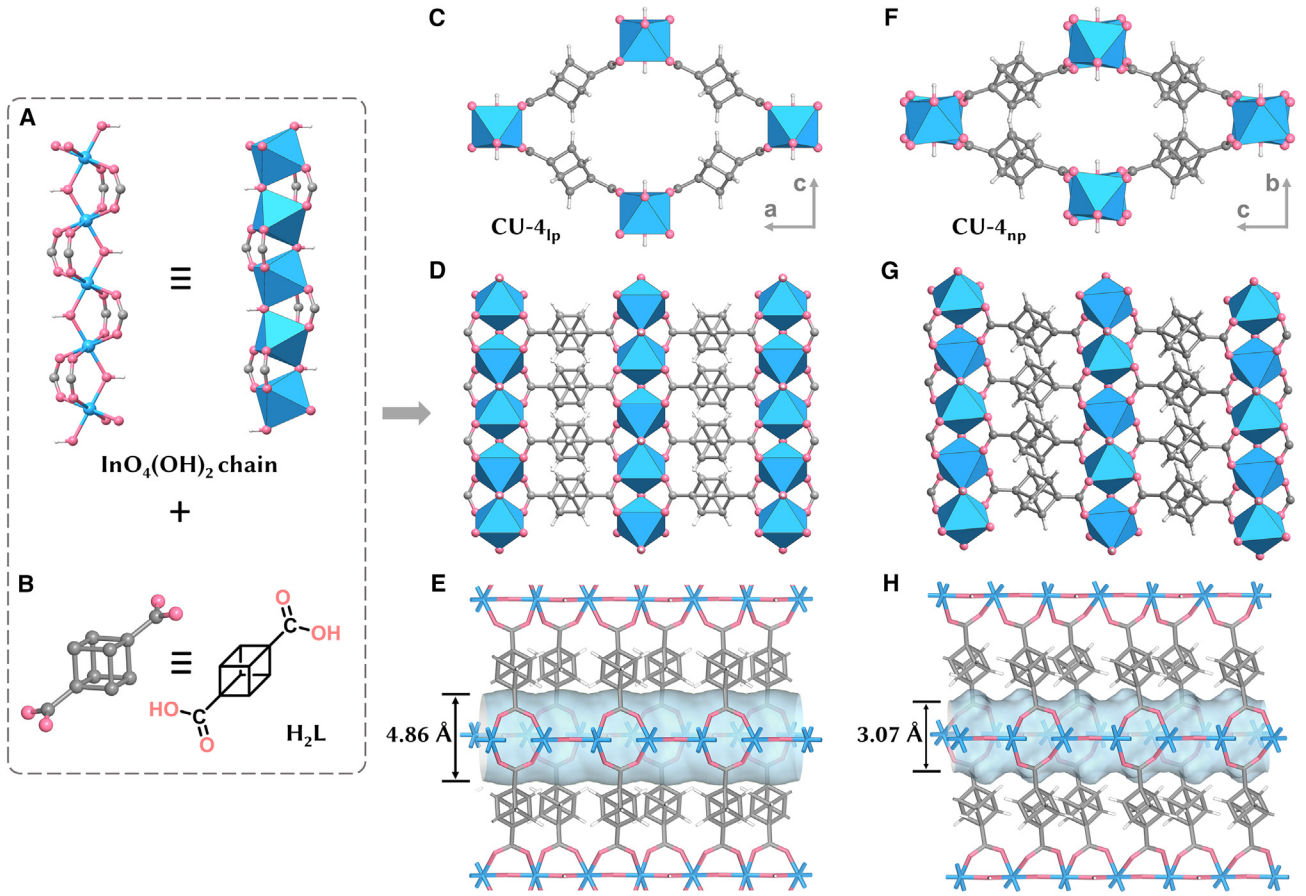

Figure 1. Structures of $CU\text{-}4_{lp}$ and $CU\text{-}4_{np}$

(A and B) Structures of the octahedral $[InO_4(OH)_2]$ chain (A) and ligand linker (B).

(C and F) Pore structures.

(D and G) Side view visualizing the arrangement of $[InO_4(OH)_2]$ chains (D) and H_2L linkers (G).

(E and H) One-dimensional channels of **$CU\text{-}4_{lp}$** (E) and **$CU\text{-}4_{np}$** (H).

Color code: In, blue octahedron; C, gray; O, pink; H, white.

solution at 120°C for either 24 or 48 h led to the formation of rod-like single crystals (Figure S1). The isolated crystals were stored in fresh DMF and denoted as **CU-4**. Synthesis of **CU-4** from 5 mL reactions up to 230 mL yielded crystals with consistent crystallinity and porosity (Figures S2 and S3). Single-crystal X-ray diffraction (SCXRD) revealed that it crystallizes in the orthorhombic space group *Imma*. As shown in Figure 1D, ligands **L** are organized into 1D stacks running parallel to the infinite $[InO_4(OH)_2]$ chains. Adjacent $[InO_4(OH)_2]$ chains and stacks of parallel ligands **L** are then arranged in parallel, thus forming one-dimensional channels along the b axis (Figures 1C, 1E, and S29). The pore-limiting diameter (PLD) and largest cavity diameter (LCD), calculated with Poreblazer and a helium probe,[46] are 4.86 and 5.29 Å, respectively (Table S5). Interestingly, we observed significant changes in the powder X-ray diffraction (PXRD) patterns (a new peak at 10.7°) when DMF was exchanged with ethanol or acetone and also when activated (Figure 2A). To explore the structure of this new phase, we conducted SCXRD on both the ethanol-exchanged and the activated **CU-4**; we observed a transition to a monoclinic *I*2/*a* space group with half **L**, half In^{3+}, and half bridging –OH in its asymmetric unit. Compared with the DMF-solvated structure, the octahedral geometry around In^{3+} and cubane skeleton within **L** is twisted (Figures 1D and 1G), resulting in a contracted, one-dimensional channel with PLD and LCD values reduced to 3.07 and 3.54 Å, respectively (Figures 1H and S30; Table S5). These findings show that **CU-4** is a flexible, three-dimensional framework composed of *trans*-corner-shared octahedral $[InO_4(OH)_2]$ chains interconnected by **L** ligands (Figures 1A and 1B) displaying a one-dimensional channel in the Z-direction (Figures 1C, 1E, 1F, and 1H).

Similar to the MIL-53 series,[47] **CU-4** exhibits a breathing effect in response to treatment variations between a large-pore and a narrow-pore configuration (Scheme 1; Figure 1). We therefore used the same terminology and named these two phases **$CU\text{-}4_{lp}$** and **$CU\text{-}4_{np}$** (lp, large pore; np, narrow pore). The experimental PXRD patterns of ethanol- and acetone-exchanged and activated **CU-4** match well with those of the simulated **$CU\text{-}4_{np}$**, confirming the phase purity of the bulk sample (Figure 2A). Furthermore, we performed Pawley refinements on the bulk

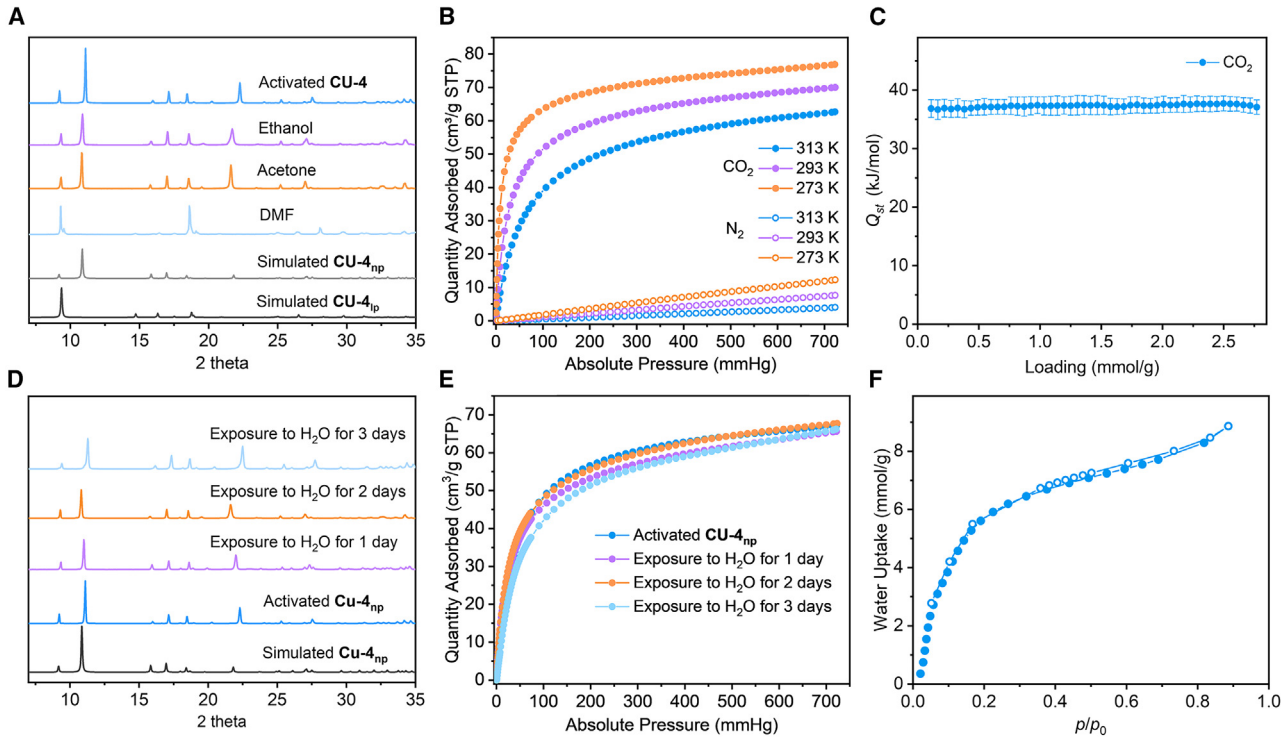

Figure 2. Characterization and adsorption performance

(A and D) PXRD patterns.

(B and E) CO_2 (B) and N_2 (E) adsorption isotherms.

(C) Isosteric heat of adsorption for the adsorption of CO_2, calculated from the isotherms measured at three temperatures.

(F) Water adsorption (solid circles) and desorption (open circles) isotherm at 298 K.

DMF-solvated **CU-4** and confirmed that the large-pore form is stable in DMF (Figure S28). The N_2 isotherm of activated **CU-4** at 77 K highlights its flexibility. As shown in Figure S4, the activated **CU-4** did not adsorb N_2 until p/p_0 approached 0.7, indicating that the material remains in the narrow-pore form, which, at 77 K, barely allows N_2 molecules to enter. There was a slight increase in N_2 uptake with increasing pressure until $p/p_0 \approx 0.9$, where a step was observed, and the N_2 uptake increased from 24 to 126 cm^3/g. This was most likely due to the partial reopening of the pore within **CU-4**. Afterward, the N_2 uptake continued to rise until it reached a maximum uptake of 137 cm^3/g at $p/p_0 \approx 0.98$. The desorption process exhibited a significant hysteresis by maintaining the high N_2 uptake down to $p/p_0 \approx 0.026$, below which the N_2 uptake sharply decreased. Unlike the flexible behavior observed from the N_2 isotherm at 77 K, the N_2 and CO_2 adsorption isotherms at 195 K did not trigger the breathing transition. Instead, they exhibited a typical type I shape with negligible hysteresis upon desorption (Figures S5 and S6), showing that, as expected, temperature plays a role in the phase transitions and scaffold rigidity at or above 195 K.

Single-component gas adsorption

To evaluate the performance of the activated structure (**CU-4np**) for carbon capture, we first conducted single-component adsorption isotherms for CO_2 and N_2 at −78°C (195 K), 0°C (273 K), 20°C (293 K), and 40°C (313 K). Prior to the measurements, the as-synthesized **CU-4** was washed with DMF, exchanged with acetone, and then evacuated under vacuum at 120°C for 14 h, resulting in activated **CU-4**. Figure 2B shows the type I adsorption isotherms obtained for both gases. In contrast to the N_2 adsorption at 77 K, there was no evidence of phase changes at the studied temperatures for either CO_2 or N_2. The CO_2 uptake reached 70 cm^3/g (3.1 mmol/g) at 1 bar and 293 K. By contrast, N_2 isotherms showed negligible uptake (7 cm^3/g at 1 bar), most likely because N_2 molecules were excluded from the pore, consistent with our initial hypothesis and PLD values calculated by Poreblazer (Table S5). Reducing the temperature to 273 K resulted in a higher CO_2 uptake, yet N_2 uptake remained minimal with ca. 12 cm^3/g (0.5 mmol/g) at 1 bar. This trend persisted even at 195 K, where CO_2 adsorption reached 83 cm^3/g (3.7 mmol/g), whereas that for N_2 reached only 4 cm^3/g (0.2 mmol/g) at 1 bar (Figures S5 and S6). Subsequently, we calculated the Q_{st} via the Clausius-Clapeyron equation for CO_2, which exhibited a flat curve across the range of loadings (Figure 2C), indicating the presence of energetically homogeneous binding sites over the loading range.[43] The zero-loading Q_{st} for CO_2 was 36.9 kJ/mol (Figure 2C), comparable to that of some other representative materials (Table S17), such as dptz-$CuSiF_6$,[43] UTSA-16,[48] and CALF-20.[4] Such moderate Q_{st} values are highly desirable when we consider lower energy requirements for material regeneration. By contrast, the Q_{st} value calculated for N_2 at zero-loading was 27.6 kJ/mol (Figure S7), lower

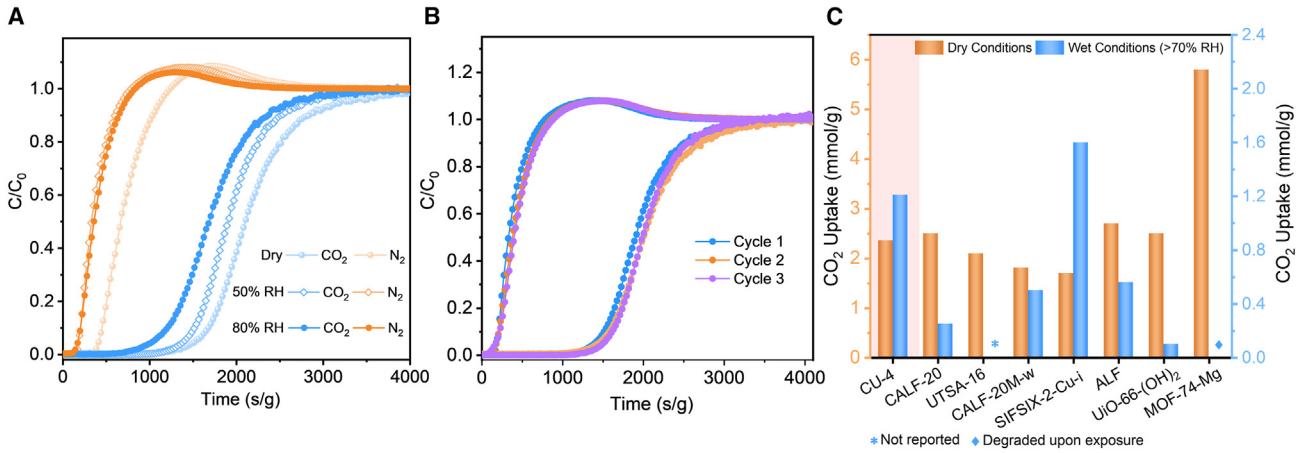

Figure 3. Breakthrough test

(A) Breakthrough curves for CO_2 and N_2 (15/85, v/v) at 293 K and 1 bar.

(B) Cyclic breakthrough separation experiments for CO_2 and N_2 (15/85, v/v) at 293 K and 1 bar under 50% RH.

(C) Performance of **CU-4** for the uptake of CO_2 under dry conditions from thermodynamic equilibrium adsorption isotherms and under wet conditions from breakthrough experiments. Performance is benchmarked against that of leading MOF-based physisorbents. The source data and supporting references are available in Table S17 and the supplemental information. Please note: the scale of the y axis for dry (left) and wet (right) conditions is different.

than that of CO_2, which further shows the presence of the relatively stronger binding interaction formed between CO_2 and **CU-4$_{np}$**. We also calculated the IAST selectivity using the DS-Langmuir and Toth models for experimental CO_2 and N_2 isotherms, respectively, to assess the adsorption selectivity (Figure S11; Table S9). Figures S9 and S10 show the calculated IAST selectivity for a binary CO_2/N_2 (15/85 and 4/96 v/v) mixture at 293 K, which gradually decreased from 236.6 and 240.2 at very low pressure to 202.2 and 197.8, respectively, at 1 bar. These results are comparable to those of benchmark materials that do not contain open metal sites or amine-based linkers, such as CALF-20 and the SIFSIX-series MOFs (Figure 3C; Table S17).[4,49]

Since most industrial process streams inevitably contain 4–20 vol % of water (e.g., coal-fired boilers, 8–10 vol %; natural-gas-fired boilers, 18–20 vol %; blast furnace gas, 4–5 vol %; cement kiln-off gas, 12.8 vol %; and oil refineries, 14–15 vol %),[50] the CO_2 uptake and selectivity against N_2 are not the only important parameters in carbon capture. In particular, one also needs to consider the MOF stability against water as well as the competitive adsorption of water versus CO_2. In the past, we have shown how physisorbent MOFs with high affinity for molecules with important electrostatic interactions, such as CO_2, will also show high affinity toward water, whereas highly hydrophobic MOFs will not adsorb water or the target adsorbate.[51] To study the water stability, we exposed **CU-4$_{np}$** to liquid water for up to 3 days. As shown in Figures 2D and 2E, both PXRD patterns and CO_2 isotherms at 293 K remained unchanged after the water treatment, indicating excellent tolerance to water. The thermogravimetric analysis (TGA) curve shows that **CU-4$_{np}$** was thermally stable until 380°C (Figure S12). Furthermore, the K-edge extended X-ray absorption fine structure (EXAFS) experiments confirmed that the local coordination environment of In^{3+} ions remained intact (Figures S13–S15; Table S10). The water adsorption isotherm of **CU-4$_{np}$** showed low uptakes of ca. 5.6, 7.6, and 8.9 mmol/g at 20, 50, and 90% RH, respectively (Figure 2F). The profile indicates that **CU-4$_{np}$** has a lower affinity for water than established water-resistant MOFs (such as MOF-74-Ni,[3] UiO-66-$(OH)_2$,[3] Al fumarate,[52] and CAU-10[53]) and comparable water uptakes with respect to contemporary MOFs (such as CALF-20, CALF-20M-w, CALF-20M-e, and NU-220[4,12]).The enhanced stability of **CU-4$_{np}$** is attributed to the presence of the infinite-chain secondary building unit (SBU) and the bulky 3D ligand. Compared with discrete SBUs, infinite-chain SBUs, such as $[InO_4(OH)_2]$ chains, have been reported to improve the hydrothermal stability of MOFs.[54,55] Moreover, in addition to facilitating angstrom-level control over pore sizes, 3D linkers (such as the 3D, cubane-derived ligand) have shown high hydrothermal stability by preventing the approach of water molecules to the metal-carboxylate coordination bonds.[56,57]

Dynamic breakthrough tests

To further evaluate the practical separation performance of simulated flue gas, we next conducted the dynamic breakthrough test at 293 K and 1 bar for binary gas mixtures of CO_2 and N_2 (15/85, v/v) under dry and wet conditions (Figure 3) with a flow rate of 6.67 cm^3/min. The analysis of performance under wet conditions was necessary given that, as described above, competitive water adsorption is a challenge in the development of new adsorbents for carbon capture. In all the breakthrough cases, N_2 eluted first from the packed column and reached saturation with negligible CO_2 detected, whereas CO_2 took a longer time to break through the column, demonstrating the capability of the framework to separate both gases. Notably, N_2 exhibited a "roll-up" behavior, typical when CO_2 displaces the small amounts of adsorbed N_2 in binary gas mixtures. In the case of dry conditions, the breakthrough times were 413 and 1,517 s/g for N_2 and CO_2, respectively, which correspond to a CO_2 adsorption capacity of 1.06 mmol/g (total effective capacity: 1.52 mmol/g). Under humid conditions at 50% RH, breakthrough times decreased to 177 and

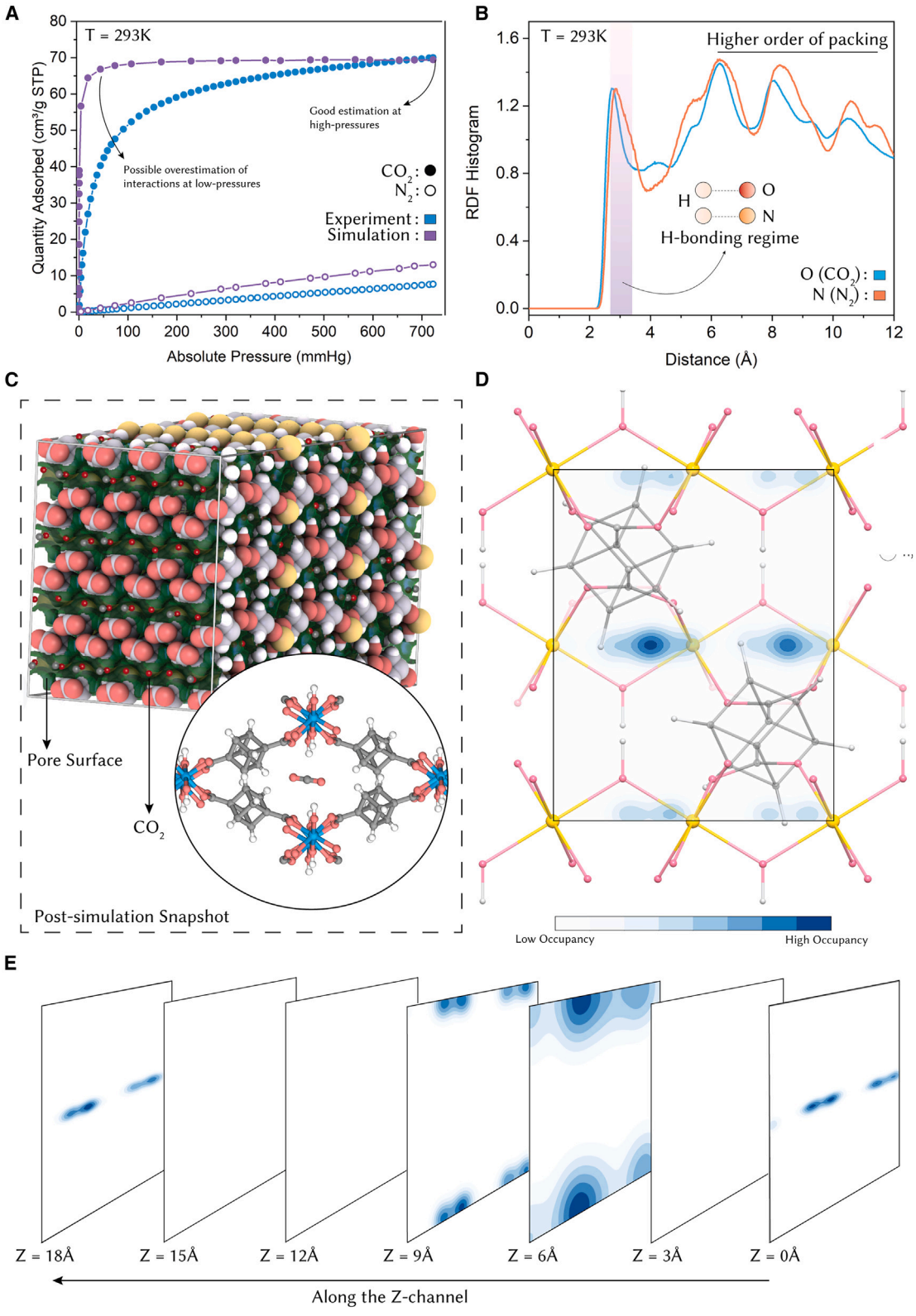

(legend on next page)

1,403 s/g for N_2 and CO_2, respectively (Figure 3A), which correspond to a CO_2 adsorption capacity of 0.97 mmol/g (total effective capacity: 1.36 mmol/g), suggesting that the presence of water competes with both N_2 and CO_2 for adsorption sites. Despite the small detrimental effect of humidity, **CU-4$_{np}$** was still able to discriminate between CO_2 and N_2 and showed a minimal impact of 7.5% reduction on the CO_2 breakthrough time, as opposed to a 57% reduction on N_2. We further evaluated the impact of the amount of water on the separation performance by increasing the humidity further. At 80% RH, the breakthrough time for CO_2 decreased from 1,517 s/g under dry conditions to 1,030 s/g, which translates to 0.73 mmol/g (total effective capacity: 1.21 mmol/g)—a 32% reduction. Overall, these findings imply that **CU-4$_{np}$** has selective adsorption properties that favor CO_2 in both dry and humid conditions, although its efficiency for CO_2 separation decreases as humidity increases (Figure 3C). In our analysis, prior to each breakthrough cycle, we regenerated **CU-4$_{np}$** by heating it to 120°C for 2 h under a flow of dry He until no detectable N_2/CO_2/water on mass spectrometry was measured. Figure 3B shows three breakthrough cycles at 293 K and 50% RH on **CU-4$_{np}$**. The sample maintained its separation performance, demonstrating excellent stability, recyclability, and durability—making it a promising candidate for physisorption-based CO_2 capture in wet flue gas streams. Figure 3C shows a comparison of **CU-4$_{np}$** benchmarked against leading MOF-based CO_2 physisorbents; Table S17 shows the values and references. To allow for a fair comparison, we took CO_2 uptake under dry conditions from thermodynamic equilibrium adsorption isotherms but took moisture adsorption capacities from dynamic, breakthrough experiments. Whereas the CO_2 uptake of **CU-4$_{np}$** was comparable to that of CALF-20,[4] UTSA-16,[48] and ALF[3] under dry conditions, notably, under humid conditions (>70% RH) most of these MOFs reported a significant drop in their CO_2 uptakes, and others, such as MOF-74-Mg, degraded upon exposure to water (Figure 3C). For instance, the CO_2 uptake of CALF-20 decreased drastically when the RH exceeded 50% and was negligible at 75% RH (it went from 2.7 mmol/g under dry conditions at 293 K and 0.15 bar to 0.25 mmol/g at 74% RH), corresponding to a 90% reduction from dry conditions.[12] By contrast, **CU-4$_{np}$**, despite a 30% drop in its uptake under wet conditions, maintained a competitive capacity for CO_2 under such conditions, second to SIFSIX-2-Cu-i (Figure 3C).

Mechanistic studies

To gain mechanistic insights into the gas adsorption process in **CU-4$_{np}$** and **CU-4$_{lp}$**, we performed atomistic grand canonical Monte Carlo (GCMC) simulations (see supplemental methods section S4 for details). We began by simulating the single-component adsorption isotherms of CO_2 and N_2 in **CU-4$_{np}$** and **CU-4$_{lp}$** at 293 K (Figures 4A and S16). The simulated results for **CU-4$_{np}$** closely matched the experimental maximum uptake for CO_2 with a small overestimation for N_2. In both cases, the host-guest interactions were overestimated, something typically found when generic force fields, such as the Dreiding and universal force field, are used (Figure 4A).[58] Overall, the simulations captured the selectivity of **CU-4$_{np}$** for CO_2 over N_2. We further simulated mixture isotherms for CO_2/N_2 (15%/85%) to study the competitive uptake of the gases. Figure S20 shows the highly selective uptake of CO_2 with negligible N_2 uptake across the pressure range studied, aligning well with the observations from the single-component gas adsorption isotherms and simulations (Figure 2B). We then calculated radial distribution functions (RDFs) (Figures 4B and S17–S19) to find how the atoms radially pack around each other.[59] Figure 4B shows the average distance between the framework H atoms from the [$InO_4(OH)_2$] chains and the O atom in CO_2 (denoted O[CO_2]) and the N atom in N_2 (denoted N[N_2]). The first peak, for both CO_2 and N_2, was observed at ~2.5 Å, which corresponds to the formation of strong H bonds,[60] whereas the peaks at a longer range imply a higher order of packing for the adsorbed molecules. The minimal distance between the In node and O[CO_2] and the node and N [N_2] corresponds to >4 Å, which is insufficient for the formation of coordination bonds (Figures S17 and S19).[61,62] **CU-4$_{np}$** was calculated to have a higher enthalpy of adsorption (ΔH_{ad}) for CO_2 (−50.69 kJ/mol) than **CU-4$_{lp}$** (−34.57 kJ/mol). This increase in the magnitude of enthalpy could be due to a greater overlap of the attractive potential fields from the opposite walls of the framework caused by the narrowing of the cavity.[49] The narrow-pore configuration of **CU-4** thus leads to more favorable interactions for CO_2 than the large-pore configuration does. This favorable uptake, however, also extends to N_2 given that **CU-4$_{np}$** had a higher enthalpy of adsorption (−25.59 kJ/mol) than **CU-4$_{lp}$** (−18.64 kJ/mol). Despite this, the magnitude of the difference is smaller for N_2 and is unable to compensate for a higher N_2 uptake (Figures 4A and S16) given that a higher selectivity was maintained in the narrow-pore configuration.

Adsorption snapshots allow us to visualize CO_2 molecules along the pore channels of **CU-4$_{np}$** and reveal that CO_2 molecules occupy the center of the pore (Figure 4C). Although snapshots provide an instantaneous view of the occupancy, they do not provide a comprehensive understanding of the distribution of CO_2 throughout the porosity and along the [In-O-In] backbone channel. To address this, we first compressed the occupancies

Figure 4. Computational insights into CO_2 adsorption by CU-4$_{np}$

(A) Comparison of experimental and simulated CO_2 and N_2 isotherms at 293 K for **CU-4$_{np}$**.

(B) Radial distribution functions (RDFs) between framework H and O(CO_2) in blue and framework H and N(N_2) in orange. Typical donor-acceptor distances for H bonds are 2.7–3.3 Å.

(C) Configuration of CO_2 molecules along the pore channels of **CU-4$_{np}$** from the single-component adsorption simulation (color code: In, yellow; O, pink; C, gray; H, white). Inset: snapshot of a single unit cell (color code: In, blue; O, pink; C, gray; H, white).

(D) Average C(CO_2) occupancy across the unit cell, viewed along the XY plane (coordinates of the supercell were folded into a single cell) (color code: In, blue; O, pink; C, gray; H, white).

(E) C(CO_2) occupancy along the pore channel. Each slice considers occupancy for a 3 Å window behind it. Blank slices indicate that there is no occupancy within the window. Note: each slice depicts the relative occupancy of the respective window.

of the center of mass (COM) of the CO_2 molecules from the simulation supercell down to a single unit cell at each cycle (i.e., a set of Monte Carlo moves; see supplemental methods section S4 for more details) after equilibration. We then performed a kernel density estimation (KDE) by using a Gaussian kernel, which helped identify regions of high occupancy within the cell and along the pore channel (Figures 4D and 4E). Because the simulation samples the free-energy landscape of the system, regions of high guest occupancy point to energetically favorable sites—i.e., "wells" in the free-energy surface.[4] In terms of absolute occupancy, as witnessed in the post-simulation snapshot (Figure 4C), the center of the pore has the most energetically favorable sites. However, certain energetically favorable sites are also present at the periphery of the cell (Figure 4D). To better understand the occupancy along the pore channel, we prepared slices by binning occupancies along a 3 Å window along the Z-channel (Figure 4E). Blank slices indicate the windows without CO_2 molecules; near the extremities of the channel, energetically favorable sites are at the center of the cell, whereas at the center of the channel, energetically favorable sites are at the periphery. It is, however, crucial to note that each slice represents a relative occupancy, i.e., the occupancy relative to the 3 Å posterior window, and not the absolute occupancy, i.e., that for the whole cell. As observed in Figure 4D, the occupancy at the center of the cell is higher, implying that the center of the cell is energetically more favorable for guest occupancy, most likely because of an overlap of H bonds between O[CO_2] and the framework H. This observation supports our framework's design rationale, where restraining the framework into a narrow pore provides a conducive environment with favorable interactions for the selective confinement of CO_2—discussed subsequently.

To gain additional insights into the competitive behavior of CO_2 with H_2O, we simulated mixture isotherms at 1 bar and varying RH. Even though these isotherms' capacity was overestimated in comparison with that of the experimental single-component water sorption isotherm (Figure 2F), which we expected given that these simulations are challenging because of the polar nature of water,[4,12] Figure S21 indicates that the H_2O uptake remained constant up to 40% RH and then gradually increased up to 80% RH, above which it saturated. Consequently, there was a gradual drop in CO_2 uptakes above 40% RH. Notably, compared with CALF-20, which reached its saturation limit at ~40% RH and then dramatically dropped in CO_2 uptake, **CU-4** reached its saturation limit at ~80% and showed reasonable CO_2 uptakes even at relatively high RH.[4] For a better understanding of the performance of **CU-4** in a real-world, post-combustion capture process, we used the machine-assisted adsorption process learning and emulation (MAPLE) framework[63] to quantitatively simulate the productivity of CO_2 separation from simulated flue gas for **CU-4** in comparison with CALF-20. MAPLE uses a four-step process comprising a feed step, a blowdown step, an evacuation step, and a light-product pressurization step. The competitive adsorption equilibrium in the MAPLE framework is assumed to be described by the single-site Langmuir (SSL) isotherm. Hence, we used the SSL model to fit experimental isotherms to compute the Langmuir adsorption parameters required for the process calculation (e.g., saturation capacity [Q_{sat}], adsorption equilibrium constant for CO_2 [b_{CO2}], adsorption equilibrium constant for N_2 [b_{N2}], heat of adsorption of CO_2 [ΔU_{CO2}], and heat of adsorption of N_2 [ΔU_{N2}]). Figures S22 and S23 show the fittings for CALF-20 and **CU-4**, respectively, and Table S14 shows the input parameters fitted to experimental pure single-component N_2 and CO_2 isotherms for **CU-4** and CALF-20 at different temperatures. Using MAPLE's implemented four-step process, we found the calculated CO_2 productivity of **CU-4** (1.62 mol $CO_2/m^3/s$) to be comparable to that of CALF-20 (1.69 mol $CO_2/m^3/s$). Here, Table S15 shows the input parameters for the simulation of the post-combustion capture process; Table S16 shows the comparison of CO_2 purity, recovery, productivity, and energy consumption for **CU-4** and CALF-20.

Guest configuration determined by *in situ* SXPD

To gain further structural insights into the flexibility of **CU-4** to variations in gas and temperature and, importantly, the configuration of gas molecules within the framework, we conducted *in situ* synchrotron X-ray powder diffraction (SXPD) experiments on the loading of CO_2, N_2, or He as a function of temperature. In brief, the activated MOF was equilibrated with 1.2 bar of CO_2, N_2, or He at 300 K. The sample was then sealed and cooled to 100 K before being warmed back to 300 K. The data were collected every 100 K (see supplemental methods for full details). Pawley refinement of the data showed no significant changes in lattice parameters, indicating the retention of the narrow-pore phase during the abovementioned treatment (Figure S27; Tables S6–S8). The diffraction peaks at 5.80° (011), 8.45° (110), and 9.04° (013) slightly shifted to higher angles as the temperature decreased. These changes reverted as the temperature increased (Figures S24–S26), suggesting reversible gas adsorption.[64]

The binding sites of CO_2 within **CU-4$_{np}$** were also determined through Rietveld refinements on SXPD data collected at 100 K. The contracted channels of **CU-4$_{np}$** were populated with two types of adsorbed CO_2 molecules (Figure 5A). Site I (0.25 CO_2 per In^{3+} center) is primarily stabilized by H bonds with the hydroxyl groups of the In-oxo chain (O–H$\cdots$O$_{CO2}$ = 2.08(2), 2.71(2) Å) and further reinforced by van der Waals (vdW) interactions with the aliphatic hydrogen centers (C–H$\cdots$O$_{CO2}$ = 3.03(3)–3.80(3) Å) (Figure 5B, left). Site II (0.33 CO_2 per In^{3+} center) is anchored close to the cubane moiety via stronger vdW interactions at shorter C–H$\cdots$O$_{CO2}$ distances of 2.11(3)–3.13(3) Å (Figure 5B, right). To complement the observations from the *in situ* data, we identified potential binding sites within the framework from the probability distributions of the CO_2 molecules obtained from GCMC simulations at 100 K (see supplemental methods sections S4 and S5 for details). The SXPD observations are consistent with the GCMC simulations, wherein the probability distributions of the COM of the CO_2 molecules after equilibration were collected and two potential binding sites, i.e., the sites with the highest relative occupancies (denoted site I* and site II*), were calculated (see supplemental methods section S5 for details). Although we would ideally expect CO_2 to be localized at a single site with small fluctuations at 100 K,[65] given the inherent noise of the Monte Carlo sampling process, and for a comparison with the SXPD data, we chose to analyze the two sites with the highest occupancies. These sites are, however, in close

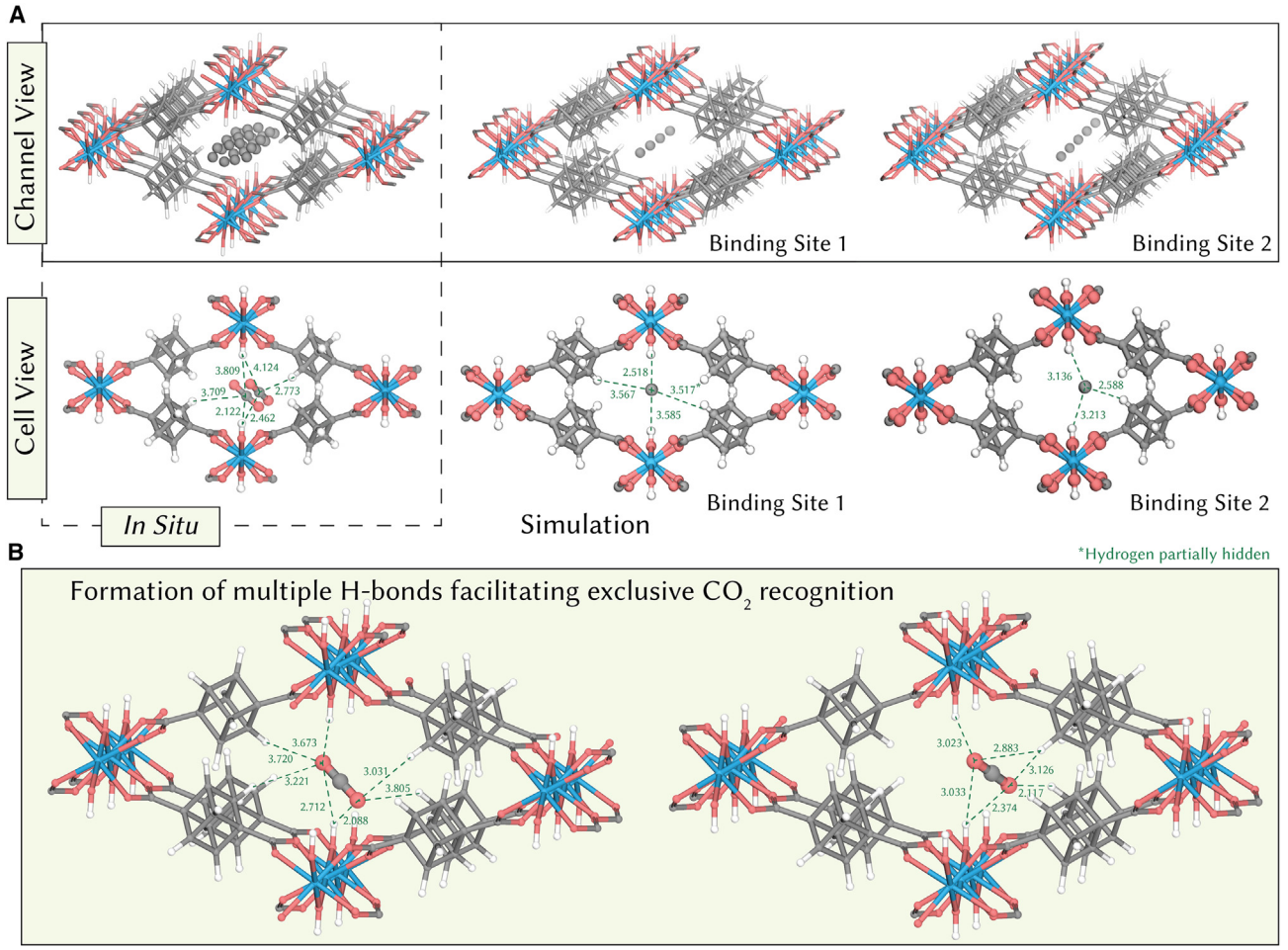

Figure 5. Configurations of adsorbed CO_2 molecules within CU-4_{np} from refinements of *in situ* SXPD data and GCMC simulations

(A) Experimentally observed and theoretically calculated CO_2 binding sites when viewed along the channel (top) and for a single unit cell (bottom).

(B) Experimentally observed binding sites provide insights into host-guest interactions, suggesting the formation of multiple H bonds and vdW interactions for the exclusive recognition of CO_2.

proximity to one another. Both site I* (having a higher relative occupancy) and site II* occupy the center of the pore along the channel, consistent with the SXPD models (Figure 5A). In cohesion with the SXPD model, the host-guest binding distances for both theoretical sites are consistent with the formation of multiple H bonds and vdW interactions (Figure 5A). These observations confirm our hypothesis that through the induction of the narrow pore, we achieved a confined pore environment that facilitates strong host-guest interactions, allowing for the selective recognition of CO_2. It is worth noting that the mechanism of CO_2 capture proposed for **CU-4_{np}**—featuring the creation of a hydrogen-confined narrow-pore cavity with multiple strong and weak interactions—deviates significantly from those observed in most other adsorbents that typically bind to CO_2 through open metal sites, via electrostatic interactions, or through chemical reactions with N_2-containing linkers.[66,67] The formation of adsorption pockets that can selectively recognize and concentrate CO_2 has been described by Zaworotko and co-workers[67] as an "enzyme-like" behavior that has previously been observed in the SIFSIX-series.[43,67] This behavior is sometimes also referred to as "hand-in-glove" binding, as observed in the case of ALF.[3] In contrast to ALF, in the case of **CU-4**, a "lock-and-key" binding is observed as a result of the frustrated-flexibility state induced by the bulky organic ligand incorporated into the structure. The lock-and-key model describes enzymes as having a fixed, rigid active (i.e., rigid-template) site that perfectly fits a specific substrate, much like a key fits into a lock. By contrast, following a (many times) more accurate description of enzymes, the "induced-fit" model—and its metaphoric hand-in-glove model—suggests that the enzyme's active site is flexible and adjusts its shape upon substrate binding to achieve a better fit.[68,69] The adsorption pocket formed, for example, in SIFSIX-18-Ni-b facilitates tight CO_2 binding via strong C···F and relatively weaker C-H···O interactions, leading to high binding interactions (Q_{st} value of 52 kJ/mol).[67] By contrast, in the case of **CU-4**, CO_2 binding occurs via multiple overlapping C–H···O and vdW interactions. Although these interactions result in tight CO_2 binding, they are weaker than those

of SIFSIX-18-Ni-b, resulting in milder interaction energies and allowing **CU-4** to maintain a high selectivity while having lower energy requirements for regeneration.

Outlook

We have reported a novel MOF, **CU-4**, featuring electron-deficient In^{3+} and a bulky 3D cubane-derived ligand containing multiple hydrogen moieties. By exploiting the structural dynamics of the framework, we were able to realize a hydrogen-confined pore cavity that is conducive to the exclusive recognition of CO_2 and validate it by experimental adsorption isotherms and molecular simulations. Moreover, because of the incorporation of the bulky ligand, once the MOF attains its narrow-pore configuration, it adopts a frustrated state, which minimizes framework dynamics during guest uptake. In its narrow-pore configuration, **CU-4** presents an ideal pore environment that can optimize host-guest interactions for a lock-and-key binding of CO_2 through multiple H bonds and weak vdW interactions, as confirmed by *in situ* synchrotron studies and computational models, demonstrating selectivity that is comparable to that of benchmark MOFs. The moderate Q_{st} for the adsorption of CO_2 allows for energy-efficient adsorption-desorption cycles that balance the strength and reversibility of the host-guest interactions. Moreover, **CU-4** displays excellent water stability in that it maintains a high selectivity for CO_2 even at high RH levels up to 80%, as well as excellent recyclability, as revealed by dynamic breakthrough tests. With performance comparable to that of contemporary benchmark materials (Figure 3C; Table S17), **CU-4** is particularly applicable for post-combustion capture. We foresee that such design strategies that leverage framework flexibility can be generalized to achieve the next generation of MOF-based sorbents for energy-efficient molecular separations that maximize both working capacity and selectivity. As we look toward industrial translation, indeed, the next frontier involves MOF production at scales compatible with industrial requirements by capitalizing on recent protocols for the large-scale synthesis of MOFs and their precursors.[70,71] Our current efforts are aimed at optimizing these synthesis routes to reduce the associated costs.

RESOURCE AVAILABILITY

Lead contact

Requests for further information and resources should be directed to and will be fulfilled by the lead contact, David Fairen-Jimenez (df334@cam.ac.uk).

Materials availability

The datasets and materials generated and/or analyzed during this study are available from the lead contact upon reasonable request.

Data and code availability

Materials synthesis, characterizations, methods, and computational details are provided in the supplemental information. The crystallography data in this work have been deposited in the Cambridge Crystallographic Data Centre (CCDC) under accession numbers CCDC: 2330360 (CU-4_{lp}), 2330361 (CU-4_{np}), 2330362 (activated CU-4), and 2351159 (CO_2@CU-4_{np}_100K). These data can be obtained free of charge from CCDC via www.ccdc.cam.ac.uk/data_request/cif.

METHODS

Detailed methods can be found in the supplemental information.

ACKNOWLEDGMENTS

This project received funding from the EPSRC (EP/S009000/1). D.M. acknowledges NanoDTC Cambridge – EPSRC EP/S022953/1. M.R.A.K. acknowledges support from the Cambridge Trust Scholarship and the Trinity Henry-Barlow Scholarship. M.A. acknowledges the ERC under the HORIZON TMA MSCA (101106377 CLARIFIER) and UKRI (EP/Y023447/1). O.K.F. is thankful for the financial support from the Paula M. Trienens Institute for Sustainability and Energy and from US Department of Energy (DOE) grant DE-FG02-08ER15967/0018. We thank the staff of PROXIMA 2A (Soleil Synchrotron, France) for assistance and acknowledge the beamtime under the standard proposal 20220874. We also thank Diamond Light Source for access to beamlines I11 (CY32566) and B18 (SP34552), especially Dr. Lucy Saunders, Dr. Sarah Day, and Dr. Luke Keenan.

AUTHOR CONTRIBUTIONS

X.C. and D.F.-J. conceived the project. X.C. designed the experiments. D.M. designed the simulations. D.M. and M.R.A.K. conducted GCMC simulations. X.C. and W.S. collected the X-ray data. X.W. and X.T. performed the breakthrough measurements. X.C., M.A., and M.R.A.K. conducted the *in situ* SXPD and *ex situ* XAS experiments. M.H. and S.Y. refined the *in situ* SXPD data. L.L.K. analyzed the XAS data. M.R.A.K. and M.A. performed adsorption process simulation. X.C. and D.M. drafted the manuscript. All authors discussed the results and commented on the manuscript.

DECLARATION OF INTERESTS

D.F.-J. has financial interests in the start-up company Immaterial, which is seeking to commercialize MOFs.

SUPPLEMENTAL INFORMATION

Supplemental information can be found online at https://doi.org/10.1016/j.chempr.2024.11.020.

Received: July 5, 2024
Revised: October 24, 2024
Accepted: November 26, 2024
Published: January 3, 2025

REFERENCES

1. Habert, G., Miller, S.A., John, V.M., Provis, J.L., Favier, A., Horvath, A., and Scrivener, K.L. (2020). Environmental impacts and decarbonization strategies in the cement and concrete industries. Nat. Rev. Earth Environ. *1*, 559–573. https://doi.org/10.1038/s43017-020-0093-3.
2. Sholl, D.S., and Lively, R.P. (2016). Seven chemical separations to change the world. Nature *532*, 435–437. https://doi.org/10.1038/532435a.
3. Evans, H.A., Mullangi, D., Deng, Z., Wang, Y., Peh, S.B., Wei, F., Wang, J., Brown, C.M., Zhao, D., Canepa, P., et al. (2022). Aluminum formate, $Al(HCOO)_3$: an earth-abundant, scalable, and highly selective material for CO_2 capture. Sci. Adv. *8*, eade1473. https://doi.org/10.1126/sciadv.ade1473.
4. Lin, J.B., Nguyen, T.T.T., Vaidhyanathan, R., Burner, J., Taylor, J.M., Durekova, H., Akhtar, F., Mah, R.K., Ghaffari-Nik, O., Marx, S., et al. (2021). A scalable metal-organic framework as a durable physisorbent for carbon dioxide capture. Science *374*, 1464–1469. https://doi.org/10.1126/science.abi7281.
5. Chen, L., Li, F., Zhang, Y., Bentley, C.L., Horne, M., Bond, A.M., and Zhang, J. (2017). Electrochemical reduction of carbon dioxide in a

monoethanolamine capture medium. ChemSusChem *10*, 4109–4118. https://doi.org/10.1002/cssc.201701075.

6. Dutcher, B., Fan, M., and Russell, A.G. (2015). Amine-based CO_2 capture technology development from the beginning of 2013 – a review. ACS Appl. Mater. Interfaces *7*, 2137–2148. https://doi.org/10.1021/am507465f.
7. Gouedard, C., Picq, D., Launay, F., and Carrette, P.L. (2012). Amine degradation in CO_2 capture. I. A review. Int. J. Greenhouse Gas Control *10*, 244–270. https://doi.org/10.1016/j.ijggc.2012.06.015.
8. Jahandar Lashaki, M., Khiavi, S., and Sayari, A. (2019). Stability of amine-functionalized CO_2 adsorbents: a multifaceted puzzle. Chem. Soc. Rev. *48*, 3320–3405. https://doi.org/10.1039/c8cs00877a.
9. Qazvini, O.T., Babarao, R., and Telfer, S.G. (2021). Selective capture of carbon dioxide from hydrocarbons using a metal-organic framework. Nat. Commun. *12*, 197. https://doi.org/10.1038/s41467-020-20489-2.
10. Shi, Y., Xie, Y., Cui, H., Ye, Y., Wu, H., Zhou, W., Arman, H., Lin, R.B., and Chen, B. (2021). Highly selective adsorption of carbon dioxide over acetylene in an ultramicroporous metal-organic framework. Adv. Mater. *33*, e2105880. https://doi.org/10.1002/adma.202105880.
11. Singh, G., Lee, J., Karakoti, A., Bahadur, R., Yi, J., Zhao, D., AlBahily, K., and Vinu, A. (2020). Emerging trends in porous materials for CO_2 capture and conversion. Chem. Soc. Rev. *49*, 4360–4404. https://doi.org/10.1039/d0cs00075b.
12. Wang, X., Alzayer, M., Shih, A.J., Bose, S., Xie, H., Vornholt, S.M., Malliakas, C.D., Alhashem, H., Joodaki, F., Marzouk, S., et al. (2024). Tailoring hydrophobicity and pore environment in physisorbents for improved carbon dioxide capture under high humidity. J. Am. Chem. Soc. *146*, 3943–3954. https://doi.org/10.1021/jacs.3c11671.
13. Sumida, K., Rogow, D.L., Mason, J.A., McDonald, T.M., Bloch, E.D., Herm, Z.R., Bae, T.H., and Long, J.R. (2012). Carbon dioxide capture in metal-organic frameworks. Chem. Rev. *112*, 724–781. https://doi.org/10.1021/cr2003272.
14. Bose, S., Sengupta, D., Rayder, T.M., Wang, X., Kirlikovali, K.O., Sekizkardes, A.K., Islamoglu, T., and Farha, O.K. (2023). Challenges and opportunities: metal–organic frameworks for direct air capture. Adv. Funct. Mater. *34*, 2307478. https://doi.org/10.1002/adfm.202307478.
15. Yao, X., Cordova, K.E., and Zhang, Y.-B. (2022). Flexible metal–organic frameworks as CO_2 adsorbents en route to energy-efficient carbon capture. Small Struct. *3*, 2100209. https://doi.org/10.1002/sstr.202100209.
16. Zhang, Z., Chen, Y., Chai, K., Kang, C., Peh, S.B., Li, H., Ren, J., Shi, X., Han, X., Dejoie, C., et al. (2023). Temperature-dependent rearrangement of gas molecules in ultramicroporous materials for tunable adsorption of CO_2 and C_2H_2. Nat. Commun. *14*, 3789. https://doi.org/10.1038/s41467-023-39319-2.
17. Smith, G.L., Eyley, J.E., Han, X., Zhang, X., Li, J., Jacques, N.M., Godfrey, H.G.W., Argent, S.P., McCormick McPherson, L.J., Teat, S.J., et al. (2019). Reversible coordinative binding and separation of sulfur dioxide in a robust metal-organic framework with open copper sites. Nat. Mater. *18*, 1358–1365. https://doi.org/10.1038/s41563-019-0495-0.
18. Adil, K., Belmabkhout, Y., Pillai, R.S., Cadiau, A., Bhatt, P.M., Assen, A.H., Maurin, G., and Eddaoudi, M. (2017). Gas/vapour separation using ultramicroporous metal-organic frameworks: insights into the structure/separation relationship. Chem. Soc. Rev. *46*, 3402–3430. https://doi.org/10.1039/c7cs00153c.
19. Ji, Z., Wang, H., Canossa, S., Wuttke, S., and Yaghi, O.M. (2020). Pore chemistry of metal–organic frameworks. Adv. Funct. Mater. *30*, 2000238. https://doi.org/10.1002/adfm.202000238.
20. Lee, J.H., Jeoung, S., Chung, Y.G., and Moon, H.R. (2019). Elucidation of flexible metal-organic frameworks: research progresses and recent developments. Coord. Chem. Rev. *389*, 161–188. https://doi.org/10.1016/j.ccr.2019.03.008.
21. Li, Y., Wang, Y., Fan, W., and Sun, D. (2022). Flexible metal-organic frameworks for gas storage and separation. Dalton Trans. *51*, 4608–4618. https://doi.org/10.1039/d1dt03842g.
22. Schneemann, A., Bon, V., Schwedler, I., Senkovska, I., Kaskel, S., and Fischer, R.A. (2014). Flexible metal-organic frameworks. Chem. Soc. Rev. *43*, 6062–6096. https://doi.org/10.1039/c4cs00101j.
23. Chanut, N., Ghoufi, A., Coulet, M.V., Bourrelly, S., Kuchta, B., Maurin, G., and Llewellyn, P.L. (2020). Tailoring the separation properties of flexible metal-organic frameworks using mechanical pressure. Nat. Commun. *11*, 1216. https://doi.org/10.1038/s41467-020-15036-y.
24. Zhang, J.-P., Zhou, H.-L., Zhou, D.-D., Liao, P.-Q., and Chen, X.-M. (2018). Controlling flexibility of metal–organic frameworks. Natl. Sci. Rev. *5*, 907–919. https://doi.org/10.1093/nsr/nwx127.
25. Zhao, P., Tsang, S.C.E., and Fairen-Jimenez, D. (2021). Structural heterogeneity and dynamics in flexible metal-organic frameworks. Cell Rep. Phys. Sci. *2*, 100544. https://doi.org/10.1016/j.xcrp.2021.100544.
26. Wang, S.M., Shivanna, M., Zheng, S.T., Pham, T., Forrest, K.A., Yang, Q.Y., Guan, Q., Space, B., Kitagawa, S., and Zaworotko, M.J. (2024). Ethane/ethylene separations in flexible diamondoid coordination networks via an ethane-induced gate-opening mechanism. J. Am. Chem. Soc. *146*, 4153–4161. https://doi.org/10.1021/jacs.3c13117.
27. Krause, S., Hosono, N., and Kitagawa, S. (2020). Chemistry of soft porous crystals: structural dynamics and gas adsorption properties. Angew. Chem. Int. Ed. *59*, 15325–15341. https://doi.org/10.1002/anie.202004535.
28. Fairen-Jimenez, D., Moggach, S.A., Wharmby, M.T., Wright, P.A., Parsons, S., and Düren, T. (2011). Opening the gate: framework flexibility in ZIF-8 explored by experiments and simulations. J. Am. Chem. Soc. *133*, 8900–8902. https://doi.org/10.1021/ja202154j.
29. Devic, T., Horcajada, P., Serre, C., Salles, F., Maurin, G., Moulin, B., Heurtaux, D., Clet, G., Vimont, A., Grenèche, J.M., et al. (2010). Functionalization in flexible porous solids: effects on the pore opening and the host-guest interactions. J. Am. Chem. Soc. *132*, 1127–1136. https://doi.org/10.1021/ja9092715.
30. Macreadie, L.K., Idrees, K.B., Smoljan, C.S., and Farha, O.K. (2023). Expanding linker dimensionality in metal-organic frameworks for sub-ångstrom pore control for separation applications. Angew. Chem. Int. Ed. *62*, e202304094. https://doi.org/10.1002/anie.202304094.
31. Idrees, K.B., Kirlikovali, K.O., Setter, C., Xie, H., Brand, H., Lal, B., Sha, F., Smoljan, C.S., Wang, X., Islamoglu, T., et al. (2023). Robust carborane-based metal-organic frameworks for hexane separation. J. Am. Chem. Soc. *145*, 23433–23441. https://doi.org/10.1021/jacs.3c04641.
32. Idrees, K.B., Li, Z., Xie, H., Kirlikovali, K.O., Kazem-Rostami, M., Wang, X., Wang, X., Tai, T.Y., Islamoglu, T., Stoddart, J.F., et al. (2022). Separation of aromatic hydrocarbons in porous materials. J. Am. Chem. Soc. *144*, 12212–12218. https://doi.org/10.1021/jacs.2c03114.
33. Smoljan, C.S., Li, Z., Xie, H., Setter, C.J., Idrees, K.B., Son, F.A., Formalik, F., Shafaie, S., Islamoglu, T., Macreadie, L.K., et al. (2023). Engineering metal-organic frameworks for selective separation of hexane isomers using 3-dimensional linkers. J. Am. Chem. Soc. *145*, 6434–6441. https://doi.org/10.1021/jacs.2c13715.
34. Sadakiyo, M., Yamada, T., Kato, K., Takata, M., and Kitagawa, H. (2016). A significant change in selective adsorption behaviour for ethanol by flexibility control through the type of central metals in a metal-organic framework. Chem. Sci. *7*, 1349–1356. https://doi.org/10.1039/c5sc03325j.
35. Schneemann, A., Vervoorts, P., Hante, I., Tu, M., Wannapaiboon, S., Sternemann, C., Paulus, M., Wieland, D.C.F., Henke, S., and Fischer, R.A. (2018). Different breathing mechanisms in flexible pillared-layered metal–organic frameworks: impact of the metal center. Chem. Mater. *30*, 1667–1676. https://doi.org/10.1021/acs.chemmater.7b05052.
36. Aljammal, N., Jabbour, C., Chaemchuen, S., Juzsakova, T., and Verpoort, F. (2019). Flexibility in metal–organic frameworks: a basic understanding. Catalysts *9*, 512. https://doi.org/10.3390/catal9060512.
37. Cockayne, E. (2017). Thermodynamics of the flexible metal-organic framework material MIL-53(Cr) from first principles. J. Phys. Chem. C

Nanomater. Interfaces *121*, 4312–4317. https://doi.org/10.1021/acs.jpcc.6b11692.

38. Thangavel, K., Folli, A., Fischer, M., Hartmann, M., Murphy, D.M., and Pöppl, A. (2024). Utilizing EPR spectroscopy to investigate the liquid adsorption properties of bimetallic MIL-53(Al/Cr) MOF. RSC Adv. *14*, 4244–4251. https://doi.org/10.1039/d3ra07952j.
39. Mowat, J.P.S., Seymour, V.R., Griffin, J.M., Thompson, S.P., Slawin, A.M.Z., Fairen-Jimenez, D., Düren, T., Ashbrook, S.E., and Wright, P.A. (2012). A novel structural form of MIL-53 observed for the scandium analogue and its response to temperature variation and CO_2 adsorption. Dalton Trans. *41*, 3937–3941. https://doi.org/10.1039/c1dt11729g.
40. Zhou, J., Ke, T., Steinke, F., Stock, N., Zhang, Z., Bao, Z., He, X., Ren, Q., and Yang, Q. (2022). Tunable confined aliphatic pore environment in robust metal-organic frameworks for efficient separation of gases with a similar structure. J. Am. Chem. Soc. *144*, 14322–14329. https://doi.org/10.1021/jacs.2c05448.
41. Zhang, Y., Yang, L., Wang, L., Duttwyler, S., and Xing, H. (2019). A microporous metal-organic framework supramolecularly assembled from a Cu^{II} dodecaborate cluster complex for selective gas separation. Angew. Chem. Int. Ed. *58*, 8145–8150. https://doi.org/10.1002/anie.201903600.
42. Xian, S., Peng, J., Pandey, H., Thonhauser, T., Wang, H., and Li, J. (2023). Robust metal–organic frameworks with high industrial applicability in efficient recovery of C_3H_8 and C_2H_6 from natural gas upgrading. Engineering *23*, 56–63. https://doi.org/10.1016/j.eng.2022.07.017.
43. Liang, W., Bhatt, P.M., Shkurenko, A., Adil, K., Mouchaham, G., Aggarwal, H., Mallick, A., Jamal, A., Belmabkhout, Y., and Eddaoudi, M. (2019). A tailor-made interpenetrated MOF with exceptional carbon-capture performance from flue gas. Chem *5*, 950–963. https://doi.org/10.1016/j.chempr.2019.02.007.
44. Hung, T.-H., Lyu, Q., Lin, L.-C., and Kang, D.-Y. (2021). Transport-relevant pore limiting diameter for molecular separations in metal–organic framework membranes. J. Phys. Chem. C *125*, 20416–20425. https://doi.org/10.1021/acs.jpcc.1c05959.
45. Pallach, R., Keupp, J., Terlinden, K., Frentzel-Beyme, L., Kloß, M., Machalica, A., Kotschy, J., Vasa, S.K., Chater, P.A., Sternemann, C., et al. (2021). Frustrated flexibility in metal-organic frameworks. Nat. Commun. *12*, 4097. https://doi.org/10.1038/s41467-021-24188-4.
46. Sarkisov, L., Bueno-Perez, R., Sutharson, M., and Fairen-Jimenez, D. (2020). Materials Informatics with PoreBlazer v4.0 and the CSD MOF Database. Chem. Mater. *32*, 9849–9867. https://doi.org/10.1021/acs.chemmater.0c03575.
47. Tang, J., Chu, Y., Li, S., Xu, J., Xiong, W., Wang, Q., and Deng, F. (2021). Breathing effect via solvent inclusions on the linker rotational dynamics of functionalized MIL-53. Chemistry *27*, 14711–14720. https://doi.org/10.1002/chem.202102419.
48. Xiang, S., He, Y., Zhang, Z., Wu, H., Zhou, W., Krishna, R., and Chen, B. (2012). Microporous metal-organic framework with potential for carbon dioxide capture at ambient conditions. Nat. Commun. *3*, 954. https://doi.org/10.1038/ncomms1956.
49. Nugent, P., Belmabkhout, Y., Burd, S.D., Cairns, A.J., Luebke, R., Forrest, K., Pham, T., Ma, S., Space, B., Wojtas, L., et al. (2013). Porous materials with optimal adsorption thermodynamics and kinetics for CO_2 separation. Nature *495*, 80–84. https://doi.org/10.1038/nature11893.
50. Siegelman, R.L., Kim, E.J., and Long, J.R. (2021). Porous materials for carbon dioxide separations. Nat. Mater. *20*, 1060–1072. https://doi.org/10.1038/s41563-021-01054-8.
51. Le, D.H., Loughan, R.P., Gładysiak, A., Rampal, N., Brooks, I.A., Park, A.-H.A., Fairen-Jimenez, D., and Stylianou, K.C. (2022). Lanthanide metal–organic frameworks for the fixation of CO_2 under aqueous-rich and mixed-gas conditions. J. Mater. Chem. A *10*, 1442–1450. https://doi.org/10.1039/D1TA09463G.
52. Coelho, J.A., Ribeiro, A.M., Ferreira, A.F.P., Lucena, S.M.P., Rodrigues, A.E., and Azevedo, D.C.S.d. (2016). Stability of an Al-fumarate MOF and its potential for CO_2 capture from wet stream. Ind. Eng. Chem. Res. *55*, 2134–2143. https://doi.org/10.1021/acs.iecr.5b03509.
53. López-Cervantes, V.B., Sánchez-González, E., Jurado-Vázquez, T., Tejeda-Cruz, A., González-Zamora, E., and Ibarra, I.A. (2018). CO_2 adsorption under humid conditions: self-regulated water content in CAU-10. Polyhedron *155*, 163–169. https://doi.org/10.1016/j.poly.2018.08.043.
54. Bosch, M., Zhang, M., and Zhou, H.-C. (2014). Increasing the stability of metal-organic frameworks. Adv. Chem. *2014*, 1–8. https://doi.org/10.1155/2014/182327.
55. Guo, Z.J., Yu, J., Zhang, Y.Z., Zhang, J., Chen, Y., Wu, Y., Xie, L.H., and Li, J.R. (2017). Water-stable In(III)-based metal-organic frameworks with rod-shaped secondary building units: single-crystal to single-crystal transformation and selective sorption of C_2H_2 over CO_2 and CH_4. Inorg. Chem. *56*, 2188–2197. https://doi.org/10.1021/acs.inorgchem.6b02840.
56. Smoljan, C.S., Snurr, R.Q., and Farha, O.K. (2024). 3-Dimensional linker-based metal–organic frameworks for sub-angstrom control and enhanced thermal stability. J. Mater. Res. *39*, 1047–1056. https://doi.org/10.1557/s43578-024-01309-5.
57. Slyusarchuk, V.D., Kruger, P.E., and Hawes, C.S. (2020). Cyclic aliphatic hydrocarbons as linkers in metal-organic frameworks: new frontiers for ligand design. ChemPlusChem *85*, 845–854. https://doi.org/10.1002/cplu.202000206.
58. Fairen-Jimenez, D., Galvelis, R., Torrisi, A., Gellan, A.D., Wharmby, M.T., Wright, P.A., Mellot-Draznieks, C., and Duren, T. (2012). Flexibility and swing effect on the adsorption of energy-related gases on ZIF-8: combined experimental and simulation study. Dalton Trans. *41*, 10752–10762. https://doi.org/10.1039/c2dt30774j.
59. Kirkwood, J.G., and Boggs, E.M. (1942). The radial distribution function in liquids. J. Chem. Phys. *10*, 394–402. https://doi.org/10.1063/1.1723737.
60. Jeffrey, G.A. (1997). An Introduction to Hydrogen Bonding (Oxford University Press).
61. Buchholz, D.B., Ma, Q., Alducin, D., Ponce, A., Jose-Yacaman, M., Khanal, R., Medvedeva, J.E., and Chang, R.P.H. (2014). The structure and properties of amorphous indium oxide. Chem. Mater. *26*, 5401–5411. https://doi.org/10.1021/cm502689x.
62. Anker, M.D., Lein, M., and Coles, M.P. (2019). Reduction of organic azides by indyl-anions. Isolation and reactivity studies of indium-nitrogen multiple bonds. Chem. Sci. *10*, 1212–1218. https://doi.org/10.1039/c8sc04078h.
63. Pai, K.N., Prasad, V., and Rajendran, A. (2020). Generalized, adsorbent-agnostic, artificial neural network framework for rapid simulation, optimization, and adsorbent screening of adsorption processes. Ind. Eng. Chem. Res. *59*, 16730–16740. https://doi.org/10.1021/acs.iecr.0c02339.
64. Baek, S.B., Moon, D., Graf, R., Cho, W.J., Park, S.W., Yoon, T.U., Cho, S.J., Hwang, I.C., Bae, Y.S., Spiess, H.W., et al. (2015). High-temperature in situ crystallographic observation of reversible gas sorption in impermeable organic cages. Proc. Natl. Acad. Sci. USA *112*, 14156–14161. https://doi.org/10.1073/pnas.1504586112.
65. Lin, L.C., Kim, J., Kong, X., Scott, E., McDonald, T.M., Long, J.R., Reimer, J.A., and Smit, B. (2013). Understanding CO_2 dynamics in metal-organic frameworks with open metal sites. Angew. Chem. Int. Ed. *52*, 4410–4413. https://doi.org/10.1002/anie.201300446.
66. Liu, J., Wei, Y., and Zhao, Y. (2019). Trace carbon dioxide capture by metal–organic frameworks. ACS Sustain. Chem. Eng. *7*, 82–93. https://doi.org/10.1021/acssuschemeng.8b05590.
67. Mukherjee, S., Sikdar, N., O'Nolan, D., Franz, D.M., Gascón, V., Kumar, A., Kumar, N., Scott, H.S., Madden, D.G., Kruger, P.E., et al. (2019). Trace CO_2 capture by an ultramicroporous physisorbent with low water affinity. Sci. Adv. *5*, eaax9171. https://doi.org/10.1126/sciadv.aax9171.

68. Koshland, D.E. (1995). The key–lock theory and the induced fit theory. Angew. Chem. Int. Ed. *33*, 2375–2378. https://doi.org/10.1002/anie.199423751.

69. Nelson, D.L., Lehninger, A.L., and Cox, M.M. (2008). Lehninger Principles of Biochemistry (Macmillan).

70. Falkiner, M.J., Littler, S.W., McRae, K.J., Savage, G.P., and Tsanaktsidis, J. (2013). Pilot-scale production of dimethyl 1,4-cubanedicarboxylate. Org. Process Res. Dev. *17*, 1503–1509. https://doi.org/10.1021/op400181g.

71. DeSantis, D., Mason, J.A., James, B.D., Houchins, C., Long, J.R., and Veenstra, M. (2017). Techno-economic analysis of metal–organic frameworks for hydrogen and natural gas storage. Energy Fuels *31*, 2024–2032. https://doi.org/10.1021/acs.energyfuels.6b02510.